Calculated barrier heights for OH + C2H2 and OH + C2H4 using unrestricted Møller–Plesset perturbation theory with spin annihilation

ARTICLE *in* JOURNAL OF THE AMERICAN CHEMICAL SOCIETY · JULY 1987

Impact Factor: 12.11 · DOI: 10.1021/ja00248a012

2 AUTHORS, INCLUDING:

Carlos P Sosa
University of Minnesota
106 PUBLICATIONS **2,821** CITATIONS

SEE PROFILE

Calculated Barrier Heights for OH + C_2H_2 and OH + C_2H_4 Using Unrestricted Møller–Plesset Perturbation Theory with Spin Annihilation

Carlos Sosa[†] and H. Bernhard Schlegel*[‡]

Contribution from the Department of Chemistry, Wayne State University, Detroit, Michigan 48202. *Received October 6, 1986*

Abstract: The reactions of OH radical with C_2H_2 and C_2H_4 have been studied with ab initio molecular orbital techniques. Reactants, loose clusters, transition structures, and products were optimized at UHF/3-21G and UHF/6-31G*. The barrier heights have been computed by using unrestricted Hartree–Fock and Møller–Plesset perturbation theory up to fourth order, including single, double, and quadruple excitations. Spin contamination in the UHF wave function has been corrected by annihilating the largest spin contaminant. The vibrational frequencies were computed by using analytical derivative methods at the UHF/3-21G level. The barrier heights for both reactions are overestimated by 7–15 kcal/mol at the UMP2, UMP3, and UMP4 levels. Annihilation of the largest spin contaminant lowers the barrier heights by 7–15 kcal/mol. Calculations at the PMP4/6-31G* level are in good agreement with the estimated experiment barrier heights.

The reactions of OH with acetylene and ethylene are known to be important in hydrocarbon combustion as well as atmospheric chemistry.[1-5] Experimental studies on OH + C_2H_2[1-12] and OH + C_2H_4[1-4,11-25] have shown that near room temperature the predominant mechanism involves the electrophilic addition of the OH radical to the π bond, forming an activated complex which can be collisionally stabilized.

$$OH + C_2H_{2n} \rightarrow C_2H_{2n}OH^* \quad (n = 1, 2) \qquad (1)$$

$$C_2H_{2n}OH^* + M \rightarrow C_2H_{2n}OH + M \qquad (2)$$

In early experimental work on OH + C_2H_2, no pressure dependence of the rate constant was found at low temperatures.[6,7] However, recent studies covering a wider range of temperature and pressure, and using flash photolysis/resonance fluorescence and laser pyrolysis/laser fluorescence techniques,[8-10] indicate that the rate constant does depend on the pressure, consistent with eq 1 and 2. Analysis of the temperature and pressure dependence yields an activation energy of 1.3 ± 0.1 kcal/mol,[9,10] based on an estimated heat of reaction of −36 ± 6 kcal/mol for OH + C_2H_2 → C_2H_2OH. At temperatures higher than 1000 K, the addition channel becomes less important because of competition from hydrogen abstraction (estimated activation energy 6–8 kcal/mol).[9,10]

The OH + C_2H_4 system has also received considerable attention.[11-25] In accord with eq 1 and 2, the rate for OH + C_2H_4 is found to be dependent on the total pressure. However, unlike addition to acetylene, a small negative activation energy has been found (−0.9 ± 0.2,[13,14] −0.7 ± 0.3,[15] −0.6 ± 0.3[16] kcal/mol). Several explanations have been given for this, including the formation of a weakly bound complex.[26] Estimates of the heat of reaction for the addition process range from −29 to −32 kcal/mol.[4,16-18] Mass spectral methods have been used to observe directly the primary adduct, C_2H_4OH, and to study its decomposition into CH_3 + CH_2O and H + CH_3CHO.[18,19] At higher temperatures, hydrogen abstraction becomes the dominant pathway (estimated activation energy ca. 3 kcal/mol).[1,24,25]

In an earlier theoretical study, Melius, Binkley, and Koszykowski[27] examined the reactions of OH with C_2H_2, C_2H_4, and HCN. Geometries were optimized at the HF/6-31G* level and energies were calculated by using fourth order unrestricted Møller–Plesset perturbation theory (UMP4/6-31G**). The heats of reaction and barrier heights were estimated by applying bond additivity corrections to the UMP4 calculations (BAC–MP4). These corrections were determined by a least-squares fit to ca. 50 molecules with well-established heats of formation. For open-shell molecules, estimated corrections for contamination from higher spin states are also included.

In previous work we have shown that the barrier heights for hydrogen addition to ethylene and formaldehyde are overestimated by 6–10 kcal/mol at the UMP4 level due to spin contamination in the UHF wave function. The difficulties in computing barrier heights with unrestricted Møller–Plesset perturbation theory can be overcome by annihilation of the largest spin contaminant. This leads to a much improved description of bond dissociation curves[28]

[†] Present address: Quantum Theory Project, University of Florida, Gainesville, Florida 32605.

[‡] Camille and Henry Dreyfus Teacher-Scholar.

(1) *Combustion Chemistry*; Gardiner, W. C., Jr., Ed.; Springer-Verlag: New York, 1984.
(2) Hucknall, D. J. *Chemistry of Hydrocarbon Combustion*; Chapman and Hall: New York, 1985.
(3) Glassman, I. *Combustion*; Academic Press: New York, 1977.
(4) Kerr, J. A.; Parsonage, M. J. *Evaluated Kinetic Data on Gas Phase Addition Reactions*; Butterworths: England, 1972.
(5) Williams, A.; Smith, D. B. *Chem. Rev.* **1970**, *70*, 267.
(6) Breen, J. E.; Glass, G. P. *Int. J. Chem. Kinet.* **1970**, *3*, 145.
(7) Pastrana, A.; Carr, R. W., Jr. *Int. J. Chem. Kinet.* **1974**, *6*, 587.
(8) Perry, R. A.; Atkinson, R. A.; Pitts, J. N., Jr. *J. Chem. Phys.* **1977**, *67*, 5577.
(9) Michael, J. V.; Nava, D. F.; Borkowski, R. P.; Payne, W. A.; Stief, I. J. *J. Chem. Phys.* **1980**, *73*, 6108.
(10) Smith, G. P.; Fairchild, P. W.; Crosley, D. R. *J. Chem. Phys.* **1984**, *81*, 2667.
(11) Smith, I. W. M.; Zellner, R. *J. Chem. Soc., Faraday Trans. 2* **1973**, *69*, 1617.
(12) Davis, D. D.; Fischer, S.; Schiff, R.; Watson, R. T.; Bollinger, W. *J. Chem. Phys.* **1975**, *63*, 1707.
(13) Greiner, N. R. *J. Chem. Phys.* **1970**, *53*, 1284.
(14) Tully, F. P. *Chem. Phys. Lett.* **1983**, *96*, 148.
(15) Atkinson, R.; Perry, R. A.; Pitts, J. N., Jr. *J. Chem. Phys.* **1977**, *66*, 1197.
(16) Zellner, R.; Lorenz, K. *J. Phys. Chem.* **1984**, *88*, 984.
(17) Howard, C. J. *J. Chem. Phys.* **1976**, *65*, 4771.
(18) Bartels, M.; Hoyerman, K.; Sievert, R. *Symp. (Int.) Combus. [Proc.]* **1982**, *19*, 61.
(19) Morris, E. D., Jr.; Stedman, D. H.; Niki, H. *J. Am. Chem. Soc.* **1971**, *93*, 3570.
(20) Morris, E. D., Jr.; Niki, H. *J. Phys. Chem.* **1971**, *75*, 3640.
(21) Lloyd, A. C.; Darnall, K. R.; Winer, A. M.; Pitts, J. N., Jr. *J. Phys. Chem.* **1976**, *80*, 789.
(22) Atkinson, R.; Darnall, K. R.; Lloyd, A. C.; Winer, A. M.; Pitts, J. N., Jr. *Adv. Photochem.* **1979**, *11*, 375.
(23) Klein, Th.; Barnes, I.; Becker, K. H.; Fink, E. H.; Zabel, F. *J. Phys. Chem.* **1984**, *88*, 5020.
(24) Bradley, J. N.; Capey, W. D.; Fair, R. W.; Pritchard, D. K. *Int. J. Chem. Kinet.* **1976**, *8*, 549.
(25) Westbrook, C. K.; Dryer, F. L.; Schug, K. P. *Symp. (Int.) Combust. [Proc.]* **1982**, *19*, 153.
(26) Singleton, D. L.; Cvetonovic, R. J. *J. Am. Chem. Soc.* **1976**, *98*, 6812. Mozurkewich, M.; Benson, S. W. *J. Phys. Chem.* **1984**, *88*, 6429, 6435.
(27) Melius, C. F.; Binkely, J. S.; Koszykowski, M. L. *8th International Symposium on Gas Kinetics*; Nottingham: England, 1984, and unpublished results.

0002-7863/87/1509-4193$01.50/0

and much better agreement between experimental and theoretical barrier heights.[29] The present study uses these same techniques to investigate the structures and energetics of the reactants, loose clusters, transition states, and radical intermediates for the reactions $OH + C_2H_2 \rightarrow C_2H_2OH$ and $OH + C_2H_4 \rightarrow C_2H_4OH$.

Method

Ab initio molecular orbital calculations were performed with the GAUSSIAN 82 system of programs.[30] The restricted Hartree–Fock method (RHF) was used for closed shell systems and the unrestricted Hartree–Fock method (UHF) for open shell systems.[31] All equilibrium geometries and transition structures were fully optimized at the Hartree–Fock level by using analytical gradient methods[32] with split-valence (3-21G)[33] and split-valence plus polarization (6-31G*)[34] basis sets. In addition, several points were calculated along the reaction paths for the OH addition by fixing the hydroxy–reactant distance, R(C–O), and minimizing the energy with respect to all other parameters. Vibrational frequencies and zero-point energies were obtained from analytical second derivatives[35] calculated at the HF/3-21G level. Electron correlation energy was calculated by using fourth order Møller–Plesset perturbation theory in the space of single, double, and quadruple excitations (MP4SDQ, frozen core).

The effects of spin contamination were examined by annihilation of the next highest spin component in the UHF wave function. In terms of the Löwdin spin projection operator[36]

$$\hat{P}_s = \prod_{k \neq s} \frac{\hat{S}^2 - k(k+1)}{s(s+1) - k(k+1)} \tag{3}$$

the projected Hartree–Fock energy can be written as

$$E_{\text{proj HHF}} = \frac{\langle \hat{P}_s \Psi_0 | \hat{H} | \hat{P}_s \Psi_0 \rangle}{\langle \hat{P}_s \Psi_0 | \hat{P}_s \Psi_0 \rangle} \tag{4}$$

Since $\hat{S}^2$ commutes with $\hat{H}$ and $\hat{P}_s$ is indempotent, the projected Hartree–Fock energy can also be written as

$$\begin{aligned} E_{\text{proj UHF}} &= \frac{\langle \Psi_0 | \hat{H} \hat{P}_s | \Psi_0 \rangle}{\langle \Psi_0 | \hat{P}_s \Psi_0 \rangle} \\ &= \langle \Psi_0 | \hat{H} | \Psi_0 \rangle + \frac{\sum_{i \neq 0} \langle \Psi_0 | \hat{H} | \psi_i \rangle \langle \psi_i | \hat{P}_s | \Psi_0 \rangle}{\langle \Psi_0 | \hat{P}_s \Psi_0 \rangle} \end{aligned} \tag{5}$$

Because the UHF wave function satisfies Brillouin's theorem and H contains only 1 and 2 operators, the summation over ψ_i can be restricted to all double excitations.

Often, the largest contribution to the spin contamination comes from only the next highest spin, i.e., $s + 1$. Under such circumstances, the full projection operator can be approximated by the first term in eq 3, $k = s + 1$. The result is no longer a projector (not idempotent) but an annihilation operator, $\hat{A}_{s+1}$, that removes the $s + 1$ spin contaminant (the denominator is chosen to ensure intermediate normalization of $\hat{A}_{s+1}\Psi_0$).

$$\hat{A}_{s+1} = \frac{\hat{S}^2 - (s+1)(s+2)}{\langle \Psi_0 | \hat{S}^2 | \Psi_0 \rangle - (s+1)(s+2)} \tag{6}$$

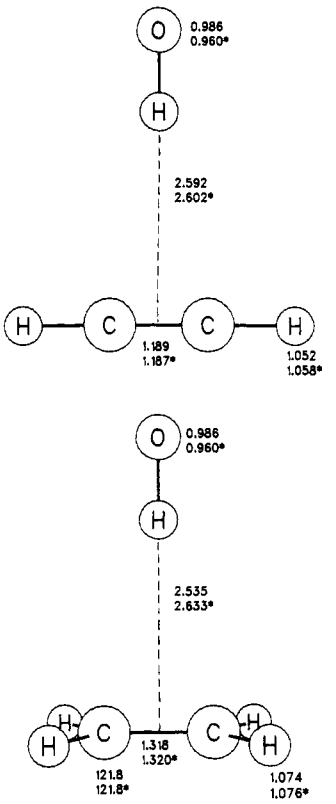

Figure 1. Geometries of the $^2B_2$ loose clusters: HF/3-21G optimized (no superscript), HF/6-31G* optimized (asterisk), in Å and deg.

This simplification was used in our first two papers,[28,29] and on the basis of eq 5 it yields the following formulae for the projected Hartree–Fock energy and wave function.

$$\begin{aligned} E_{\text{PUHF}} &= \langle \Psi_0 | \hat{H} | \Psi_0 \rangle + \frac{\sum_{i \neq 0} \langle \Psi_0 | \hat{H} | \psi_i \rangle \langle \psi_i | \hat{A}_{s+1} | \Psi_0 \rangle}{\langle \Psi_0 | \hat{A}_{s+1} | \Psi_0 \rangle} \\ &= \langle \Psi_0 | \hat{H} | \Psi_0 \rangle + \frac{\sum_{i \neq 0} \langle \Psi_0 | \hat{H} | \psi_i \rangle \langle \psi_i | \hat{S}^2 | \Psi_0 \rangle}{\langle \Psi_0 | \hat{S}^2 | \Psi_0 \rangle - (s+1)(s+2)} \\ &= E_{\text{UHF}} + \Delta E_{\text{PUHF}} \end{aligned} \tag{7}$$

$$\hat{A}_{s+1}\Psi_0 = \Psi_0 + \frac{\sum_{i \neq 0} \psi_j \langle \psi_j | \hat{S}^2 | \Psi_0 \rangle}{\langle \Psi_0 | \hat{S}^2 | \Psi_0 \rangle - (s+1)(s+2)} = \Psi_0 + \tilde{\Psi}_1 \tag{8}$$

For $\tilde{\Psi}_1$, ψ_j runs over all single excitations and all $\alpha\beta$-type double excitations.

Perturbation corrections for electron correlation, Ψ_1, Ψ_2, etc., consist of single, double, and higher excitations. As a first approximation to spin-projected UMPn energies, the spin correction $\tilde{\Psi}_1$ must be reduced by the amount already contained in Ψ_1, Ψ_2, etc. This leads to the following approximate formulae for the projected MPn energies.

$$E_{\text{PMP2}} = E_{\text{UMP2}} + \Delta E_{\text{PUHF}} \left\{ 1 - \frac{\langle \tilde{\Psi}_1 | \Psi_1 \rangle}{\langle \tilde{\Psi}_1 | \tilde{\Psi}_1 \rangle} \right\} \tag{9}$$

$$E_{\text{PMP3}} = E_{\text{UMP3}} + \Delta E_{\text{PUHF}} \left\{ 1 - \frac{\langle \tilde{\Psi}_1 | \Psi_1 + \Psi_2 \rangle}{\langle \tilde{\Psi}_1 | \tilde{\Psi}_1 \rangle} \right\} \tag{10}$$

$$\begin{aligned} E_{\text{PMP4}} &= E_{\text{UMP4}} + \Delta E_{\text{PUHF}} \left\{ 1 - \frac{\langle \tilde{\Psi}_1 | \Psi_1 + \Psi_2 + \Psi_3 \rangle}{\langle \tilde{\Psi}_1 | \tilde{\Psi}_1 \rangle} \right\} \\ &\approx E_{\text{UMP4}} + \Delta E_{\text{PUHF}} \left\{ 1 - \frac{\langle \tilde{\Psi}_1 | \Psi_1 + \Psi_2 \rangle}{\langle \tilde{\Psi}_1 | \tilde{\Psi}_1 \rangle} \right\} \end{aligned} \tag{11}$$

(28) Schlegel, H. B. *J. Chem. Phys.* **1986**, *84*, 4530.
(29) Sosa, C.; Schlegel, H. B. *Int. J. Quantum Chem.* **1986**, *29*, 1001.
(30) Binkely, J. S.; Frisch, M. J.; DeFrees, D. J.; Raghavachari, K.; Whiteside, R. A.; Schlegel, H. B.; Fluder, E. M.; Pople, J. A. GAUSSIAN 82; Carnegie-Mellon University: Pittsburgh, 1983.
(31) Pople, J. A.; Nesbet, R. K. *J. Chem. Phys.* **1954**, *27*, 571.
(32) Schlegel, H. B. *J. Comput. Chem.* **1982**, *3*, 214.
(33) Binkely, J. S.; Pople, J. A.; Hehre, W. J. *J. Am. Chem. Soc.* **1980**, *102*, 939.
(34) Hehre, W. J.; Ditchfield, R.; Pople, J. A. *J. Chem. Phys.* **1972**, *56*, 2257. Hariharan, P. C.; Pople, J. A. *Chem. Phys. Lett.* **1972**, *66*, 217.
(35) Pople, J. A.; Krishnan, R.; Schlegel, H. B.; Binkley, J. S. *Int. Quantum Chem., Quantum Chem. Symp.* **1979**, *13*, 225.
(36) Löwdin, P.-O. *Phys. Rev.* **1955**, *97*, 1509.

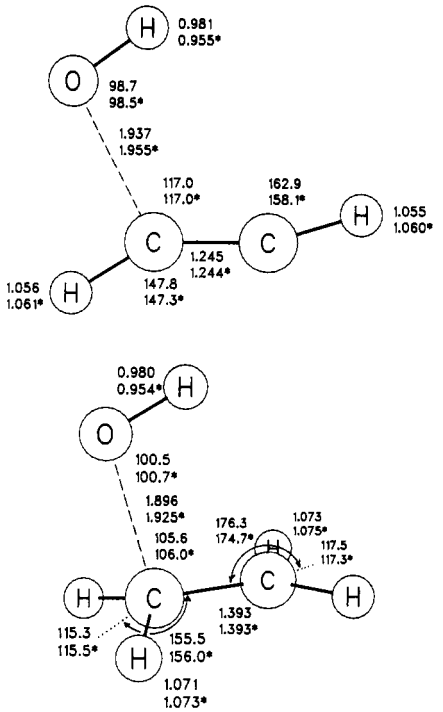

Figure 2. Geometries of the OH + C_2H_2 and OH + C_2H_4 transition states: HF/3-21G optimized (no superscript), HF/6-31G* optimized (asterisk), in Å and deg.

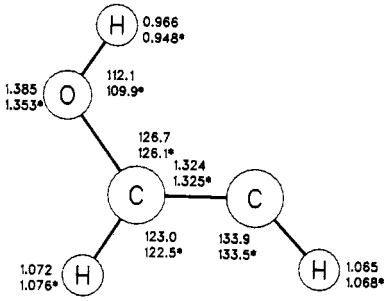

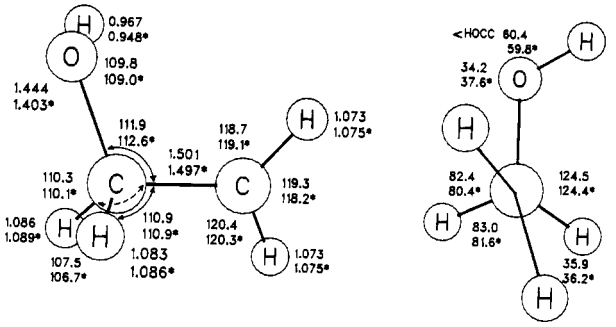

Figure 3. Geometries of 2-hydroxyethyl and 2-hydroxyethynyl radicals: HF/3-21G optimized (no superscript), HF/6-31G* optimized (asterisk), in Å and deg.

Results and Discussion

Geometry. The optimized geometries at the Hartree–Fock level for the loose clusters, transition structures, and radical intermediates are collected in Figures 1–3. Preliminary calculations on these two systems showed that the minimum energy path is one in which the OH radical is located in the symmetry plane that passes through both carbon atoms in ethylene or acetylene. Within C_s symmetry, OH can approach these molecules with the hydrogen syn or anti to the CC bond. The anti approach leads to a local maxima with two imaginary frequencies, while the syn approach corresponds to the saddle point with only one imaginary frequency. Relative to the reactants, the HF/6-31G* optimized values for

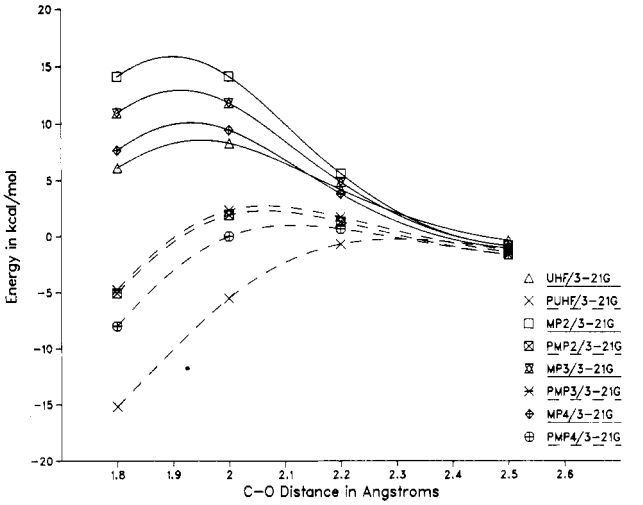

Figure 4. Energy profiles along the reaction path for addition of OH + C_2H_2 computed with the 3-21G basis set.

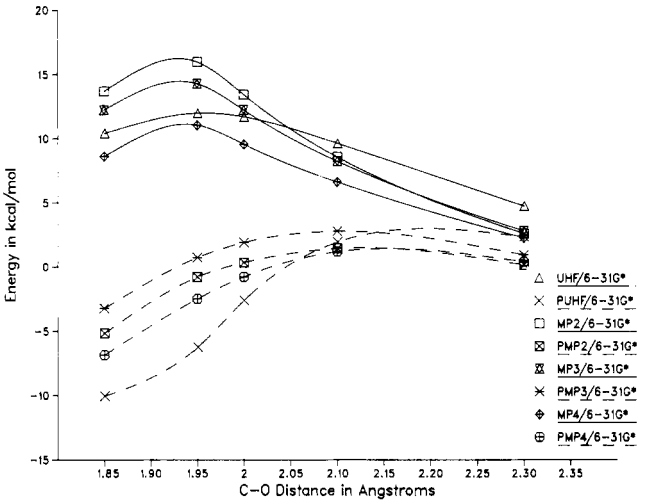

Figure 5. Energy profiles along the reaction path for addition of OH + C_2H_2 computed with the 6-31G* basis set.

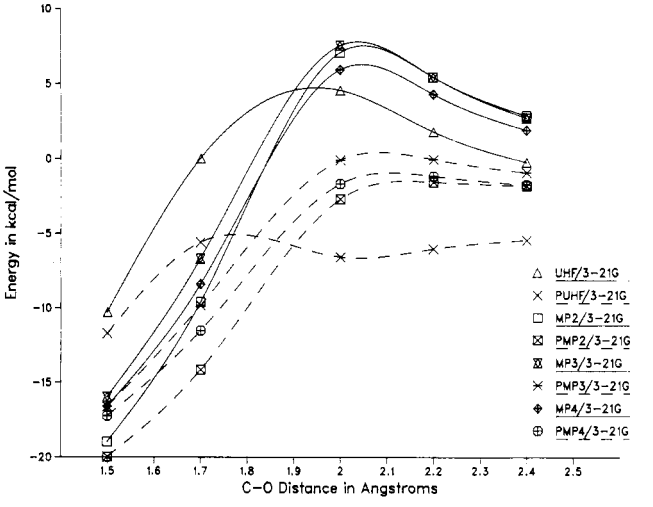

Figure 6. Energy profiles along the reaction path for addition of OH + C_2H_4 computed with the 3-21G basis set.

R(CC), R(CH), and R(OH) in the transition structure differ by only 5%, 0.3%, and −0.4%, respectively, for OH + C_2H_2 and 6%, −0.3%, and −0.6% for OH + C_2H_4. This small perturbation of the geometrical parameters at the saddle point relative to the reactants suggests that the transition structures at the Hartree–Fock level are located relatively early in the entrance channel.

Table I. Vibrational Frequencies[a,b]

structures	frequencies (cm^{-1})
	Minima
OH	3609 (3735)
C_2H_2	902 (612), 918 (729), 2234 (1974)
	3596 (3282), 3719 (3373)
C_2H_4	944 (826), 1115 (949), 1157 (943),
	1165 (1023), 1387 (1220),
	1522 (1342), 1640 (1444),
	1842 (1630), 3238 (3026),
	3305 (3021), 3371 (3103),
	3404 (3105)
C_2H_2OH	432, 517, 706, 903, 925, 1115
	1363, 1451, 1631, 3347, 3460, 3890
C_2H_4OH	215, 372, 435, 525, 908, 993
	1117, 1195, 1293, 1488, 1525, 1576
	1675, 3182, 3219, 3300, 3412, 3862
	Transition Structures
$OH + C_2H_2 \rightarrow HOCHCH$	5981, 165, 293, 413, 636, 786
	877, 974, 1682, 3545, 3599, 3697
$OH + C_2H_4 \rightarrow HOCH_2CH_2$	556i, 97, 304, 474, 820, 895
	982, 1042, 1091, 1271, 1361, 1620
	1673, 3303, 3337, 3388, 3426, 3690
	Loose Clusters
$OH + C_2H_2 \rightarrow OH\cdots C_2H_2$	66, 100, 272, 293, 901, 915
	917, 925, 2224, 3587, 3616, 3710
$OH + C_2H_4 \rightarrow OH\cdots C_2H_4$	71, 107, 108, 298, 363, 942
	1131, 1169, 1171, 1388, 1517, 1639
	1829, 3307, 3326, 3379, 3401, 3606

[a] Experimental values in parentheses from ref 43. [b] The zero-point energies in (kcal/mol) at the HF/3-21G level are the following: OH (5.2), C_2H_2 (18.9), C_2H_4 (34.6), C_2H_2OH (28.2), C_2H_4OH (43.3), OH + C_2H_2 transition structure (23.8), OH + C_2H_4 transition structure (41.1), OH + C_2H_2 cluster (25.1), and OH + C_2H_4 cluster (41.1).

In order to study the effect of electron correlation and spin contamination on the position of the transition structures, several points along the reaction path were optimized at the Hartree–Fock level, followed by single point calculations at the UMPn and PMPn levels. The results are plotted in Figures 4–7. Correlation corrections appear to displace the transition structure by 0.01–0.03 Å toward a later transition state for OH + C_2H_2, but 0.1–0.3 Å toward an earlier transition structure for OH + C_2H_4. For both systems annihilation of the largest spin contaminant shifts the transition structure by about 0.10–0.25 Å toward the reactants.

Two different loose clusters were optimized for both OH + C_2H_2 and OH + C_2H_4 (Figure 1). The binding energies are small and the monomer geometries are essentially unperturbed. For each system the $^2B_1$ and $^2B_2$ states are nearly identical in energy and structure, differing only in the orientation of the half-filled π orbital of the hydroxy. Although the $^2B_1$ states are 0.1–0.3 kcal/mol more stable, the $^2B_2$ states correlate with the $^2A'$ electronic configurations of the transition structures. The structures of the OH + C_2H_2 and OH + C_2H_4 clusters closely resemble hydrogen fluoride complexes with acetylene and ethylene, which have been studied both experimentally[37-39] and theoretically.[40,41]

Several conformations of the radical intermediates were examined. Structures I–IV represent the four different planar conformations for the C_2H_2OH radical. The optimized geometries are very similar to vinyl radical[42] and vinyl alcohol.[43] Structures II and IV are local maxima with imaginary frequencies of 65i and 47i cm^{-1} corresponding to OH torsion. Structures I and III

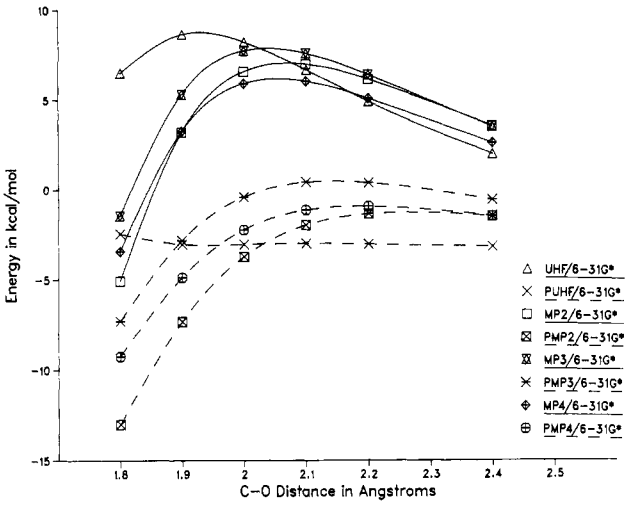

Figure 7. Energy profiles along the reaction path for addition of OH + C_2H_4 computed with the 6-31G* basis set.

Table II. Total Energies for Reactants, Clusters, and Products of the OH + C_2H_2 System[a]

level	reactants[b]	cluster[c,d]	products
	Without Spin Projection		
UHF/3-21G	−151.366 18	−151.370 19	−151.397 72
MP2/3-21G	−151.631 96	−151.636 14	−151.657 86
MP3/3-21G	−151.642 86	−151.646 96	−151.670 80
MP4/3-21G	−151.652 31	−151.656 27	−151.681 99
UHF/6-31G*	−152.200 11	−152.204 09	−152.242 91
MP2/6-31G*	−152.585 27	−152.590 31	−152.633 86
MP3/6-31G*	−152.607 61	−152.612 52	−152.654 04
MP4/6-31G*	−152.614 54	−152.619 25	−152.662 72
	After Annihilation of the Largest Spin Contaminant		
PUHF/3-21G	−151.367 12	−151.371 10	−151.411 00
PMP2/3-21G	−151.632 62	−151.636 77	−151.669 78
PMP3/3-21G	−151.643 30	−151.647 36	−151.680 44
PMP4/3-21G	−151.652 74	−151.656 68	−151.691 64
PUHF/6-31G*	−152.202 75	−152.206 71	−152.254 99
PMP2/6-31G*	−152.586 76	−152.591 77	−152.644 65
PMP3/6-31G*	−152.608 41	−152.613 30	−152.662 70
PMP4/6-31G*	−152.615 35	−152.620 02	−152.671 38

[a] Energy in au. [b] Total energies for reactants with the 6-31G** basis: HF = −152.210 16, MP2 = −152.611 38, MP3 = −152.634 65, and MP4 = −152.641 05. [c] $^2B_2$ state, geometry optimized at UHF/6-31G*. [d] Total energies for the loose cluster with the 6-31G** basis: HF = −152.214 03, MP2 = −152.616 15, MP3 = −152.639 28, and MP4 = −152.645 48.

both are local minima with III more stable than I by 1 kcal/mol at the HF/3-21G level. For 2-hydroxyethyl radical, structure V is a local maximum (OH torsion, 311i cm^{-1}); structure VI also corresponds to a maximum (CH_2 torsion, 56i cm^{-1}). Similar to the FCH_2CH_2 radical,[44] the minimum for $HOCH_2CH_2$ corresponds to a gauche conformation of the CH_2 group, as indicated in structure VI and Figure 3 (CH_2 torsion 215 cm^{-1} and OH torsion 372 cm^{-1}).

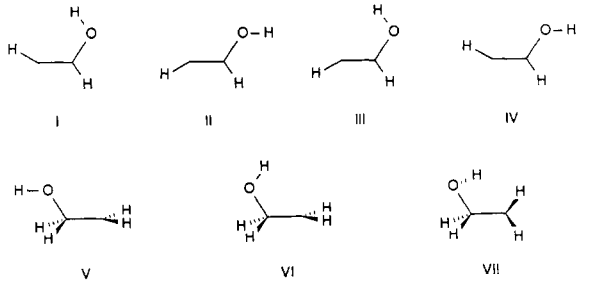

(37) Read, W. G.; Flygare, W. H. *J. Chem. Phys.* **1982**, *76*, 2238.
(38) Shea, J. A.; Flygare, W. H. *J. Chem. Phys.* **1982**, *76*, 4857.
(39) Nelson, D. D., Jr.; Fraser, G. T.; Klemperer, W. *J. Chem. Phys.* **1985**, *82*, 4483.
(40) Pople, J. A.; Frisch, M. J.; Del Bene, J. E. *Chem. Phys. Lett.* **1982**, *91*, 185.
(41) Frisch, M. J.; Pople, J. A.; Del Bene, J. E. *J. Chem. Phys.* **1983**, *78*, 4063.
(42) Dupuis, M.; Wendoloski, J. J. *J. Chem. Phys.* **1984**, *80*, 5696.
(43) Stull, D. R.; Prophet, H. *JANAF Thermochemical Tables*; U.S. Government Printing Offices: Washington DC, 1971, and subsequent supplements.
(44) Bouma, W. J.; Radom, L.; Rodwell, W. R. *Theor. Chim. Acta* **1980**, *56*, 149.

Table III. Total Energies for Reactants, Clusters, and Products of the OH + C_2H_4 System[a]

level	reactants[b]	cluster[c,d]	products
	Without Spin Projection		
UHF/3-21G	−152.571 22	−152.576 61	−152.591 65
MP2/3-21G	−152.835 32	−152.840 55	−152.868 43
MP3/3-21G	−152.858 44	−152.863 46	−152.886 93
MP4/3-21G	−152.867 02	−152.871 86	−152.896 14
UHF/6-31G*	−153.414 00	−153.418 38	−153.443 28
MP2/6-31G*	−153.804 98	−153.810 45	−153.855 68
MP3/6-31G*	−153.837 91	−153.843 12	−153.881 19
MP4/6-31G*	−153.845 09	−153.850 09	−153.888 45
	After Annihilation of the Largest Spin Contaminant		
PUHF/3-21G	−152.572 15	−152.577 11	−152.594 36
PMP2/3-21G	−152.835 98	−152.841 18	−152.870 29
PMP3/3-21G	−152.858 87	−152.863 86	−152.888 12
PMP4/3-21G	−152.867 46	−152.872 26	−152.897 33
PUHF/6-31G*	−153.416 64	−153.421 00	−153.446 35
PMP2/6-31G*	−153.806 47	−153.811 90	−153.857 65
PMP3/6-31G*	−153.838 71	−153.843 90	−153.882 38
PMP4/6-31G*	−153.845 89	−153.850 87	−153.889 64

[a] Energy in au. [b] Total energies for reactants with the 6-31G** basis: HF = −152.883 94, MP2 = −152.848 72, MP3 = −152.883 94, and MP4 = −152.889 99. [c] $^2B_2$ state, geometry optimized at UHF/6-31G*. [d] Total energies for the loose cluster with the 6-31G** basis: HF = −152.431 46, MP2 = −152.853 89, MP3 = −152.888 83, and MP4 = −152.894 67.

Table IV. Heats of Reaction[a]

level	OH + C_2H_2	OH + C_2H_4
UHF/3-21G	−19.79	−12.82
MP2/3-21G	−16.25	−20.78
MP3/3-21G	−17.53	−17.88
MP4/3-21G	−18.62	−18.27
PUHF/3-21G	−27.54	−13.94
PMP2/3-21G	−23.32	−21.53
PMP3/3-21G	−23.31	−18.35
PMP4/3-21G	−24.41	−18.74
UHF/6-31G*	−26.86	−18.37
MP2/6-31G*	−30.49	−31.81
MP3/6-31G*	−29.14	−27.16
MP4/6-31G*	−30.23	−27.21
PUHF/6-31G*	−32.78	−18.64
PMP2/6-31G*	−36.33	−32.12
PMP3/6-31G*	−34.07	−27.40
PMP4/6-31G*	−35.16	−27.45
ΔZPE[b]	4.10	3.50
exptl[c] Δ*H*(0 K)	−34 ± 5	−31 ± 5

[a] In kcal/mol. [b] At the UHF/3-21G level. [c] Reference 10.

Frequencies. The HF/3-21G harmonic frequencies are collected in Table I and are compared with experimental (anharmonic) frequencies,[45] where available. The computed frequencies are ca. 10–15% too high due to basis set effects and due to neglect of vibrational anharmonicity and electron correlation.[46,47] The low imaginary frequency of the transition structures for OH adding to acetylene and ethylene indicates a relatively flat potential energy surface for the entrance channel, consistent with Figures 4–7. Because spin projection shifts both transition states to much earlier positions along the reaction coordinate, the actual transition-state frequencies will probably be more reactant like, and the zero point energy corrections to the barriers will be much smaller or negligible.

Heats of Reaction. The total energies for reactants and products are collected in Tables II and III; the heats of reaction are summarized in Table IV. Inspection of the data indicates that enlarging the basis set (3-21G to 6-31G*) increases the stability of the two radical intermediates (C_2H_2OH and C_2H_4OH) by ca. 5–15 kcal/mol. Electron correlation contributions increase the exothermicity of the reactions by an additional 6 kcal/mol. The heats of reaction predicted at the MP4/6-31G* level are −30.2 kcal/mol for the OH + C_2H_2 system and −27.2 kcal/mol for OH + C_2H_4. Because of greater spin contamination, spin projection stabilized C_2H_2OH (S^2 = 0.992) more than C_2H_4OH (S^2 = 0.763). Changes in zero-point energy contribute 4.1 and 3.5 kcal/mol to Δ*H*(0 K) for OH + C_2H_2 → C_2H_2OH and OH + C_2H_4 → C_2H_4OH, respectively.

Estimates of the experimental heat of reaction for OH + C_2H_2 → C_2H_2OH include −30,[8] −36 ± 6,[9] and −34 ± 5[10] kcal/mol. The present calculations at the PMP4/6-31G* level (corrected for zero-point vibrational energy) predict −31.0 kcal/mol. This agrees well with the experimental extimates and with −33.2 kcal/mol calculated by Melius, Binkley, and Koszykowski[27] using the BAC–MP4 approach. For OH + C_2H_4, the experimental estimates for the heat of reaction are −29,[17] −31,[10] and −32 kcal/mol.[1,4] At the PMP4/6-31G*+ZPE level, the heat of reaction is computed to be significantly less exothermic, −24.0 kcal/mol. This smaller value is supported by the BAC–MP4 calculations[27] (−24.9 kcal/mol), which use a quite different approach to correct the energies. However, a more detailed analysis using a larger basis set and relying on isodesmic reactions favors −29 kcal/mol.[48]

The cluster well depths are summarized in Table V. Enlarging the basis set increases the binding energy by only a few tenths

Table V. Cluster Well Depths[a]

level	OH + C_2H_2	OH + C_2H_4
UHF/3-21G	2.52	3.13
MP2/3-21G	2.62	3.28
MP3/3-21G	2.57	3.15
MP4/3-21G	2.48	3.03
UHF/6-31G*	2.50	2.75
MP2/6-31G*	3.16	3.43
MP3/6-31G*	3.08	3.27
MP4/6-31G*	2.96	3.14
UHF/6-31G*	2.43	2.70
MP2/6-31G**	2.99	3.24
MP3/6-31G**	2.91	3.07
MP4/6-31G**	2.78	2.94
PUHF/3-21G	2.50	3.11
PMP2/3-21G	2.60	3.26
PMP3/3-21G	2.55	3.13
PMP4/3-21G	2.47	3.01
PUHF/6-31G*	2.48	2.74
PMP2/6-31G*	3.14	3.41
PMP3/6-31G*	3.07	3.26
PMP4/6-31G*	2.93	3.13
ΔZPE[b]	1.00	1.30

[a] $^2B_2$ state; energies in kcal/mol. [b] Calculated at the UHF/3-21G level.

Table VI. Relative Energies of OH Addition to C_2H_2 with 3-21G Basis Sets[a]

	R =						
level	1.50	1.60	1.80	2.00	2.20	2.50	2.70
	Without Spin Projection						
UHF/3-21G	−15.00	−7.47	6.15	8.33	4.15	−0.39	−1.70
MP2/3-21G	−13.22	−6.38	14.14	14.14	5.59	−0.87	−2.34
MP3/3-21G	−14.37	−7.69	10.96	11.80	4.83	−0.87	−2.24
MP4/3-21G	−16.06	−9.91	7.72	9.46	3.78	−1.09	−2.30
	After Annihilation of the Largest Spin Contaminant						
PUHF/3-21G	−23.87	−18.51	−15.16	−5.50	−0.70	−1.26	−1.90
PMP2/3-21G	−21.28	−16.34	−5.05	1.90	1.31	−1.68	−2.55
PMP3/3-21G	−20.96	−15.79	−4.73	2.33	1.71	−1.45	−2.39
PMP4/3-21G	−22.66	−18.02	−7.98	−0.01	0.65	−1.68	−2.45

[a] Energies in kcal/mol.

(45) Schlegel, H. B. *J. Phys. Chem.* **1982**, *86*, 4878.
(46) Pople, J. A.; Schlegel, H. B.; Krishnan, R.; DeFrees, D. J.; Binkley, J. S.; Frisch, M. J.; Whiteside, R. A.; Hout, R. F.; Hehre, W. J. *Int. J. Quantum Chem., Quantum Chem. Symp.* **1981**, *15*, 269.
(47) Yamaguchi, Y.; Schaefer, H. F., III *J. Chem. Phys.* **1980**, *73*, 2310.
(48) Sosa, C.; Schlegel, H. B. *J. Am. Chem. Soc.*, in press.

Table VII. Relative Energies of OH Addition to C_2H_2 with 6-31G* Basis Sets[a]

level	R = 1.85	1.95	2.00	2.10	2.30	2.50	2.70
Without Spin Projection							
UHF/6-31G*	10.42	11.99	11.70	9.63	4.73	1.44	−0.35
MP2/6-31G*	13.69	15.98	13.43	8.56	2.59	−0.42	−1.75
MP3/6-31G*	12.24	14.28	12.24	8.23	2.80	−0.16	−1.54
MP4/6-31G*	8.60	11.06	9.56	6.62	2.25	−0.32	−1.57
After Annihilation of the Largest Spin Contaminant							
PUHF/6-31G*	−10.03	−6.23	−2.60	1.94	2.35	0.71	−0.55
PMP2/6-31G*	−5.16	−0.78	0.34	1.44	0.14	−1.36	−2.11
PMP3/6-31G*	−3.22	0.73	1.91	2.79	0.92	−0.93	−1.86
PMP4/6-31G*	−6.85	−2.48	−0.77	1.19	0.38	−1.09	−1.88

[a] Energies in kcal/mol.

Table VIII. Relative Energies of OH Addition to C_2H_4 with 3-21G Basis Sets[a]

level	R = 1.50	1.70	2.00	2.20	2.40	2.70	2.75
Without Spin Projection							
UHF/3-21G	−10.25	0.02	4.56	1.80	−0.25	−1.63	−1.73
MP2/3-21G	−18.96	−9.60	7.05	5.41	2.85	0.17	−0.13
MP3/3-21G	−15.96	−6.70	7.51	5.41	2.70	0.04	−0.25
MP4/3-21G	−16.59	−8.40	5.90	4.27	1.88	−0.41	−0.65
After Annihilation of the Largest Spin Contaminant							
PUHF/3-21G	−11.70	−5.59	−6.59	−6.04	−5.47	−4.22	−3.99
PMP2/3-21G	−19.97	−14.14	−2.72	−1.58	−1.84	−2.20	−2.22
PMP3/3-21G	−16.61	−9.83	−0.11	−0.07	−0.96	−1.79	−1.86
PMP4/3-21G	−17.23	−11.53	−1.71	−1.19	−1.78	−2.24	−2.25

[a] Energies in kcal/mol.

Table IX. Relative Energies of OH Addition to C_2H_4 with 6-31G* Basis Sets[a]

level	R = 1.80	1.90	2.00	2.10	2.20	2.40	2.70
Without Spin Projection							
UHF/6-31G*	6.53	8.68	8.26	6.71	4.94	2.01	−0.36
MP2/6-31G*	−5.06	3.21	6.60	7.02	6.16	3.58	0.45
MP3/6-31G*	−1.45	5.32	7.76	7.62	6.41	3.53	0.37
MP4/6-31G*	−3.41	3.26	5.93	6.06	5.10	2.62	−0.08
After Annihilation of the Largest Spin Contaminant							
PUHF/6-31G*	−2.44	−3.03	−3.02	−2.97	−3.02	−3.15	−2.76
PMP2/6-31G*	−12.99	−7.33	−3.71	−1.96	−1.34	−1.46	−2.13
PMP3/6-31G*	−7.30	−2.82	−0.39	0.43	0.39	−0.55	−1.76
PMP4/6-31G*	−9.26	−4.88	−2.22	−1.12	−0.92	−1.46	−2.21

[a] Energies in kcal/mol.

of a kcal/mol. Previous theoretical studies on similar complexes[40,41] indicate that further increase in the basis set size will contribute less than 0.5 kcal/mol. Correlation corrections appear to change the binding energy by only 0.1–0.5 kcal/mol. Effects due to spin contamination are negligible.

Barrier Heights. The experimental activation energies are 1.3 kcal/mol for OH + C_2H_2 and −0.9 kcal/mol for OH + C_2H_4.[9,10,13-16] Since the barrier heights are correlated with the activation energies, this would indicate that the experimental classical barrier heights are approximately 1 ± 2 and 0 ± 1 kcal/mol, respectively.[49] The theoretical data are collected in Tables VI–IX and ploted in Figures 4–7. At the UHF/3-21G level, the barrier heights are overestimated by 7 kcal/mol for OH + C_2H_2 and 5 kcal/mol for OH + C_2H_4. The addition of d orbitals to the basis set (3-21G to 6-31G*) increases the barrier heights by ca. 4 kcal/mol.

Because corrections for electron correlation and spin projection change and the position of the barriers, the barrier heights at the MPn and PMPn levels must be obtained by interpolation. This can be done graphically with Figures 4–7 or numerically with the data in Tables VI–IX. The interpolated barrier heights are summarized in Table X. For OH + C_2H_2 correlation corrections make the agreement with experiment worse, raising the barrier by as much as 7 kcal/mol. For OH + C_2H_4, the barriers at the correlated levels occur considerably earlier along the reaction path and are somewhat narrower. Correlation corrections with the 6-31G* basis improve the barrier heights only slightly.

Table X. Interpolated Barrier Heights[a]

level	OH + C_2H_2	OH + C_2H_4
UHF/3-21G	8.3	4.6
MP2/3-21G	15.2	7.6
MP3/3-21G	12.4	7.8
MP4/3-21G	9.7	6.4
PUHF/3-21G	0.2	−4.5
PMP2/3-21G	2.6	−1.5
PMP3/3-21G	3.0	0.0
PMP4/3-21G	0.7	−1.2
UHF/6-31G*	12.0	8.7
MP2/6-31G*	16.3	7.0
MP3/6-31G*	14.5	8.0
MP4/6-31G*	11.2	6.1
PUHF/6-31G*	2.4	
PMP2/6-31G*	1.6	−1.2
PMP3/6-31G*	2.8	0.5
PMP4/6-31G*	1.6	−0.9
experiment	1.3 ± 0.1[b]	−0.9 ± 0.3[c]

[a] In kcal/mol. [b] References 9 and 10. [c] References 13–16.

Spin projection results in significant changes in the shapes of the potential energy curves and a remarkable improvement in the barrier heights: a decrease of 8–15 kcal/mol for OH + C_2H_2 and 7–9 kcal/mol for OH + C_2H_4. As noted before, the PUHF barriers and potential energy curves are generally not realistic.[28,29,50] However, the shapes of the PMP2, PMP3, and PMP4 curves are quite reasonable and yield very similar barriers.[51] The barriers are much lower and wider than at the unprojected levels and occur earlier along the reaction path. At the PMP4/6-31G* level, the barriers are 1.6 kcal/mol for OH + C_2H_2 and −0.9 kcal/mol for OH + C_2H_4. If transition-state theory is used to estimate the activation energies, the calculated activation energies at 298 K are 2.3 kcal/mol for OH + C_2H_2 and 0.1 kcal/mol for OH + C_2H_4 at the PMP4/6-31G* level,[52] in good agreement with the experimental activation energies, 1.3 ± 0.1 and −0.9 ± 0.3 kcal/mol, respectively. Larger basis sets, more extensive treatment of correlation corrections, full optimization of the transition structures at a spin projected level, and the use of variation transition-state theory can be expected to further improve the agreement with experiment.

Conclusions

Barrier heights for OH + C_2H_2 and OH + C_2H_4 are too high at the UHF and UMPn levels because of spin contamination. Annihilation of the largest spin contaminant shifts the barriers toward the reactants by 0.1–0.3 Å and lowers the barriers by 7–15 kcal/mol. When corrections for spin projection are combined with electron correlation corrections, good agreement with the experimental activation energies is obtained. In addition to transition states, loose clusters were found for both OH + C_2H_2 and OH + C_2H_4.

Acknowledgment. This work was supported by a grant from the National Science Foundation (Grant No. CHE-83-12505).

(49) Truhlar, D. G., private communication.

(50) Mayer, I. *Adv. Quantum Chem.* **1980**, *12*, 189.

(51) Annihilation of the higher spin contaminants caused no significant changes in the positions, shapes, and heights of the barriers at the PMPn/3-21G level.

(52) Frequencies and thermal corrections were calculated at the HF/3-21G level with the HF/3-21G optimized structure at R = 2.2 Å (i.e., near the positions of the maxima in the PMP4 curves). The OH torsion modes have been treated as free rotors in the computation of the activation energies.